Applied Physics A (2020)126:216
https://doi.org/10.1007/s00339-020-3392-0

Applied Physics A
Materials Science & Processing

Fabrication of ON/OFF switching response based on n-Ni-doped MoO_3/p-Si junction diodes using Ni-MoO_3 thin films as n-type layer prepared by JNS pyrolysis technique

M. Balaji[1] · J. Chandrasekaran[2] · M. Raja[3] · R. Marnadu[2] · M. Ramamurthy[2] · Mohd. Shkir[4,5]

Received: 31 August 2019 / Accepted: 8 February 2020

Abstract
The influence of nickel (Ni) doping concentrations on structural, optical, electrical and diode properties of molybdenum trioxide (MoO_3) thin films has been studied systematically. Ni-doped MoO_3 films and diodes were prepared for various doping concentrations of Ni such as 0, 3, 6 and 9 wt.% by jet nebulizer spray (JNS) pyrolysis technique. The structural properties of Ni-doped MoO_3 films were analyzed by X-ray diffraction (XRD) pattern and scanning electron microscopy (SEM). The prepared films were exhibited in the orthorhombic crystal structure and sub-microsized plate-like surface morphology. The energy-dispersive X-ray spectroscopy (EDX) analysis confirmed the presence of Ni, Mo and O elements in the prepared films. Ultraviolet–visible (UV–vis) analysis results showed that the absorbance decreases with the increasing of Ni doping concentration and the minimum band gap energy ($E_g = 2.25$) was obtained for 9 wt.% Ni-doped MoO_3 film. From current–voltage (I–V) characterization, the conductivity is increased by increasing the Ni doping concentration in MoO_3 thin films. The diode measurements were performed in darkness and under light illumination of a halogen lamp. The methods of I–V, Cheung's and Norde were used to calculate the diode parameters of ideality factor (n), barrier height (Φ_b) and sheet resistance (R_s). Also, the light ON/OFF switching response of the fabricated n-$NiMoO_3$/p-Si diodes was analyzed.

Keywords Ni doped MoO_3 films · I–V characterization · n-$NiMoO_3$/p-si diode · JNS pyrolysis · Ideality factor

1 Introduction

In recent years, thin-film technology is a fast-growing field for numerous industrial applications such as solar cell, diodes, gas sensors, electro and photochromic and batteries [1–6] through the transition metal oxide (TMO) of MoO_3. There are a number of TMOs existing in recent researches in which the MoO_3 thin films exhibit an attractive structural, electrical and mechanical properties. The three common phases of orthorhombic (α), monoclinic (β) and hexagonal (h) are found in MoO_3, in which α phase is thermodynamically stable one [7, 8].

The deposition methods are the most important area to grow a uniform and high-quality thin film. Nowadays a number of methods have been developed by many researchers. A few essential methods are spin coating, spray pyrolysis, thermal evaporation, and chemical vapor deposition [9–12]. Among them, we have used modified spray pyrolysis that was named as a jet nebulizer spray (JNS) pyrolysis [13–15], which is a low-cost and promising method to prepare a high-quality and uniform thin films.

✉ J. Chandrasekaran
jchandaravind@yahoo.com

[1] Department of Physics, Bannari Amman Institute of Technology, Sathyamanglam, Tamil Nadu 638401, India

[2] Department of Physics, Sri Ramakrishna Mission Vidyalaya College of Arts and Science, Coimbatore, Tamil Nadu 641020, India

[3] Vivekanandha College of Arts and Sciences for Women, Tiruchengode, Tamil Nadu 637205, India

[4] Advanced Functional Materials and Optoelectronics Laboratory (AFMOL), Department of Physics, College of Science, King Khalid University, P.O. Box 9004, Abha 61413, Saudi Arabia

[5] Research Center for Advanced Materials Science (RCAMS), King Khalid University, P.O. Box 9004, Abha 61413, Saudi Arabia

Published online: 20 February 2020

In this manuscript, the Ni doped MoO_3 thin films and n-Ni doped MoO_3/p-Si junction diodes were prepared for different doping concentrations of Ni (0, 3, 6 and 9 wt.%) at the substrate temperature of 500 °C by JNS pyrolysis technique. The prepared films were analyzed for the structural, optical and electrical properties. Significant diode parameters of ideality factor (n), barrier height (Φ_b) and sheet resistance (R_s) were calculated using different methods such as I–V, Cheung's and Norde. In addition, the switching properties of the n-Ni doped MoO_3/p-Si junction diodes were studied under dark and light condition using halogen lamp.

2 Experimental procedure

2.1 Fabrication of Ni-doped MoO_3 films and p–n junction diodes

Ammonium hepta molybdate (AHM) ($(NH_4)_6Mo_7O_{24}\bullet_4H_2O$) is the source material for MoO_3 and nickel (II) chloride ($NiCl_2\bullet6H_2O$) is used as a dopant material; both were purchased from Sigma-Aldrich and Merck. Both the materials of AHM (0.05 M) and $NiCl_2\bullet6H_2O$ (0, 3, 6 and 9 wt.%) were mixed in deionized water and stirred for an hour at ambient conditions. The well-cleaned glass substrates (2 × 2.5 cm size) were used to prepare the Ni-doped MoO_3 thin films using 3 ml of the prepared solution by JNS pyrolysis at an optimized substrate temperature of 500 °C in the air.

For fabricating a quality p–n diode, the processing of silicon wafer cleaning is the most important one for removing the impurities on the surface such as dust, grease, metallic impurities and organic residues. The cleaning process of Si wafer has been reported already [14]. The precursor solution, prepared by the mole concentration of AHM (0.05 M) and different weight percentage of $NiCl_2.6H_2O$ (0, 3, 6 and 9 wt.%), 1.5 ml was sprayed on the Boron-doped p-Si wafer (1 × 1 cm size) at the substrate temperature of 500 °C. The Si wafers have a resistivity of 0–60 Ω-cm and thickness about 279 (∓ 25) µm. Also, the orientation of the Si wafers is (100). After n-Ni doped MoO_3/p-Si diodes were fabricated, contacts were prepared on both surfaces of the diodes using the silver (Ag) paste for I–V measurements [15]. The contacts were dried at ambient conditions for 5 h. We use Ag paste for contacts on both sides of the diode because of its good properties of adhesion, high conductivity and good solderability. The experimental setup of the JNS pyrolysis technique was described in previous reports [13, 14].

2.2 Characterization

The UV–visible spectrophotometer (Perkin Elmer Lambda 35) in the wavelength range from 300 to 900 nm examined the optical properties. The X-ray diffractometer (XRD, XPERT-PRO) with CuKα1 radiation of wavelength 1.5406 Å at a generator setting of 30 mA and 40 kV in the 2θ range from 20 to 70° was used to study the structure of the Ni-doped MoO_3 films. The surface morphological changes of the coated films were observed by the scanning electron microscope (JEOL JEM 2100). The Energy Dispersive Analysis by X-ray Spectroscopy (EDX) (QUANTA FEG 250) confirms the presence of elements. For the DC electrical conductivity and diode parameters of the Ni-doped MoO_3 films, the measurement was taken using two probes by the Keithley Electrometer (6517-B).

3 Results and discussion

3.1 Optical properties

Thickness of the films plays a significant role in the film properties and electrical parameters. The thickness of the prepared films was measured by Stylus Profiler (Mitutoyo SJ 301). Thickness of the pure MoO_3 films is around 206 nm as mentioned also in our previous work [14]. The measured thickness of the doped films is 195, 216 and 220 nm for 3, 6 and 9 wt.% of Ni, respectively. The absorbance spectra of the Ni-doped MoO_3 films for different doping concentrations of Ni (0, 3, 6 and 9 wt.%) deposited at an optimized substrate temperature of 500 ºC are shown in Fig. 1a. From Fig. 1a, we observe that the increasing of the doping concentration of Ni shows the decreasing nature of absorbance. Therefore, 9% of the Ni-doped MoO_3 film shows the minimum absorbance in the UV–visible region. The Ni doping concentration gives the changes in the density of the unsaturated bonds, which resulted from the deviations in the density of localized states [16]. This may be the reason for the decrease in absorbance with Ni doping concentration. Also, the increased film thickness at higher doping concentration may have caused the reduction of absorbance. From the UV–visible spectra, the following relation (1) is used to calculate the band gap energy (E_g) of the Ni-doped MoO_3 films [15, 17, 18]:

$$\alpha h\upsilon^n = B(h\upsilon - E_g) \tag{1}$$

The plot of $(\alpha h\nu)^2$ versus $(h\nu)$ for the Ni-doped MoO_3 films is attained from Fig. 1b. The direct allowed transition is confirmed by the straight line portion. The band gap energy values of 2.50, 2.68, 2.37 and 2.25 eV for different Ni doping concentrations of 0, 3, 6 and 9 wt. % of Ni-doped MoO_3 films are taken from the extrapolation of the vertical straight line of the plot to the photon energy axis (i.e., x-axis). The minimum band gap energy is obtained for 9 wt.% of Ni-doped MoO_3 films. By increasing the carrier density, the shifting of energy band with some of the Mo^{6+} ions replaced by Ni^{2+} ions resulted in a slight shift of the

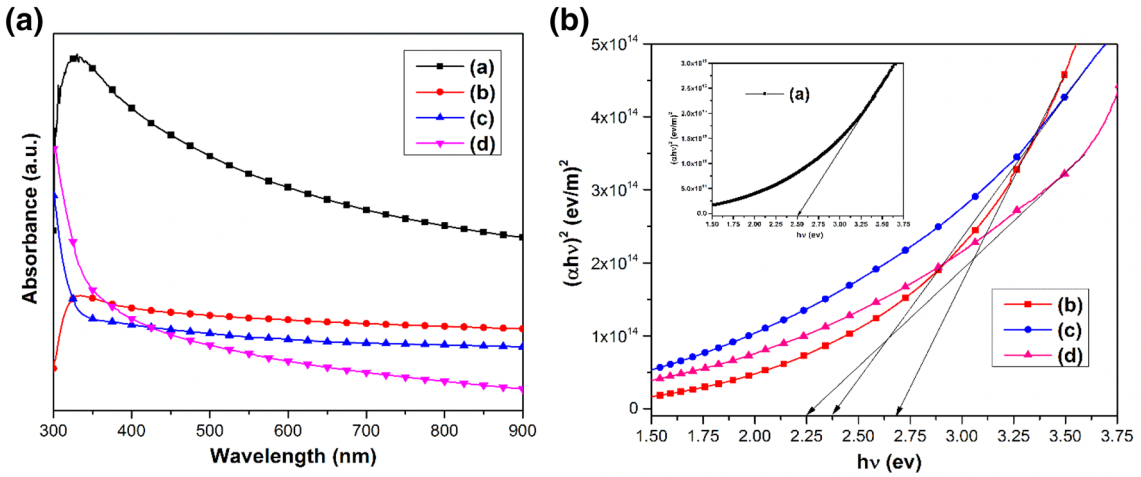

Fig. 1 **a** Absorbance spectra and **b** Band gap energy for (**a**) 0, (**b**) 3, (**c**) 6 and (**d**) 9 wt.% of Ni-doped MoO_3 thin films

Fermi level into the conduction band. The band gap mainly depends on the excitation of electrons to the Fermi level of conduction band from the valance band [19–21].

3.2 Structural study

Ni-doped MoO_3 thin films were prepared for different doping concentrations of Ni and their structural properties were studied using XRD pattern, which is shown in Fig. 2a. From the XRD pattern, the $NiMoO_3$ films are showing the polycrystalline nature with a preferred orientation of (0 4 0) plane and the diffraction angle (2θ) of 25.5°. Other diffraction peaks of 2θ in degree with the function of (*h k l*) planes relate to 23.2 (1 1 0), 27.3 (0 2 1), 33.6 (1 1 1), 35.4 (0 4 1), 38.8 (1 3 1), 46.2 (0 6 1), 49.1 (0 0 2), 52.7 (2 1 1), 55.1 (1 1 2), 58.8 (0 8 1), 64.5 (0 6 2) and 67.4 (2 6 1). From Fig. 2a, the observed diffraction peaks confirm the orthorhombic structure of MoO_3 (JCPDS card no. 35-0609). The intensity of the preferred orientation of (0 4 0) is decreased by increasing of Ni doping concentration. Figure 2b is drawn between the diffraction peaks of 25.3° and 25.8° for identifying the shift of the peaks owing to increasing the Ni doping. However, by increasing the Ni doping concentration, we observe no other peaks for Ni in the prepared films using JNS technique. The result may be due to that the very minimum concentration of nickel may be present as a small cluster on MoO_3 lattice, so the Ni phase might be

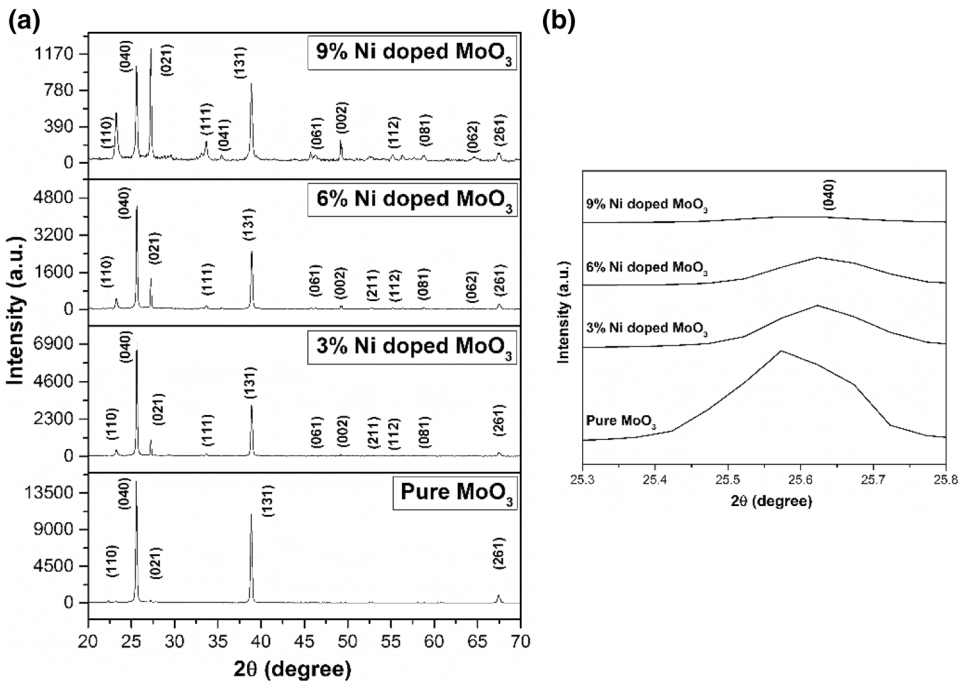

Fig. 2 **a** XRD pattern of $NiMoO_3$ thin films for different doping concentrations of Ni. **b** The shift in diffraction angle of 2θ (°) between 25.3 and 25.8

difficult to identify using X-Ray diffraction instruments. And another reason may be that the Ni impurities possibly located in the grain boundaries or dispersed in the lattices of the MoO_3 films [22–24].

The microstructural properties of pure and $NiMoO_3$ thin films for the preferred orientation of (0 4 0) plane are shown in Table 1. The crystallite size (D) [25, 26], dislocation density (δ), microstrain (ε) and stacking fault (SF) values are calculated by the following relations (2–5) [14, 15, 17]:

$$D = \frac{k\lambda}{\beta\cos\theta}, \tag{2}$$

$$\varepsilon = \frac{\beta\cos\theta}{4}, \tag{3}$$

$$\delta = \frac{1}{D^2}, \tag{4}$$

$$\mathrm{SF} = \left[\frac{2\pi^2}{45(3\tan\theta)^{1/2}}\right]\beta, \tag{5}$$

where 'k'—shape factor ($k = 0.94$), 'λ'—wavelength of the X-ray radiation, 'θ'—diffraction angle and 'β'—full width at half maximum.

From Fig. 3a, as the Ni concentration increases from 0 to 9 wt.%, the crystallite size (D) for the preferred orientation of (0 4 0) plane is decreased from 55.26 to 41.45 nm and microstrain increased from 0.62 to 0.83×10^{-3} lines^{-2} m^{-4} (Table 1), which may be owing to the ionic radius difference between Ni and Mo. From Table 1, the other properties of dislocation density (Fig. 3b) and stacking fault of pure and $NiMoO_3$ films are increased by increasing Ni doping concentration. Madhavi et al. [27] and Lethy et al. [28] also discussed that the crystallite size decreases with increasing the doping concentrations.

3.3 Surface morphology

Figure 4a–d shows the surface morphological images of the pure and Ni-doped MoO_3 films. From Fig. 4, the increasing of the doping concentration of Ni (0, 3, 6 and 9 wt.%) varies the morphology of the films. Figure 4a and b shows the sub-microsized plate-like structures, which are randomly oriented. From Fig. 4c, 6 wt.% of Ni doping has highly varied the morphology of $NiMoO_3$ film that is an agglomeration of plates with rod-like structures. Figure 4d depicts the morphology of 9 wt.% of Ni doped MoO_3 thin film, which shows the agglomerated sub-microsized plate-like structure. It should be mentioned that the plate-like structure effectively

Table 1 The microstructural properties of $NiMoO_3$ films

Ni doping concentration (wt. %)	Diffraction angle 2θ (deg)	(040) Inter planar distance Å	FWHM (Radians)	Crystallite size (D) nm	Micro strain (ε) (× 10^{-3} lines^{-2} m^{-4})	Dislocation density (× 10^{14} lines/m^2)	Stacking fault × 10^{-2}
0	25.5845	3.4815	0.00257	55.26	0.6277	3.2747	0.1353
3	25.6333	3.4750	0.00260	55.20	0.6280	3.2751	0.1355
6	25.6029	3.4791	0.00268	55.06	0.6300	3.2800	0.1454
9	25.6289	3.4756	0.00343	41.45	0.8370	5.8207	0.1806

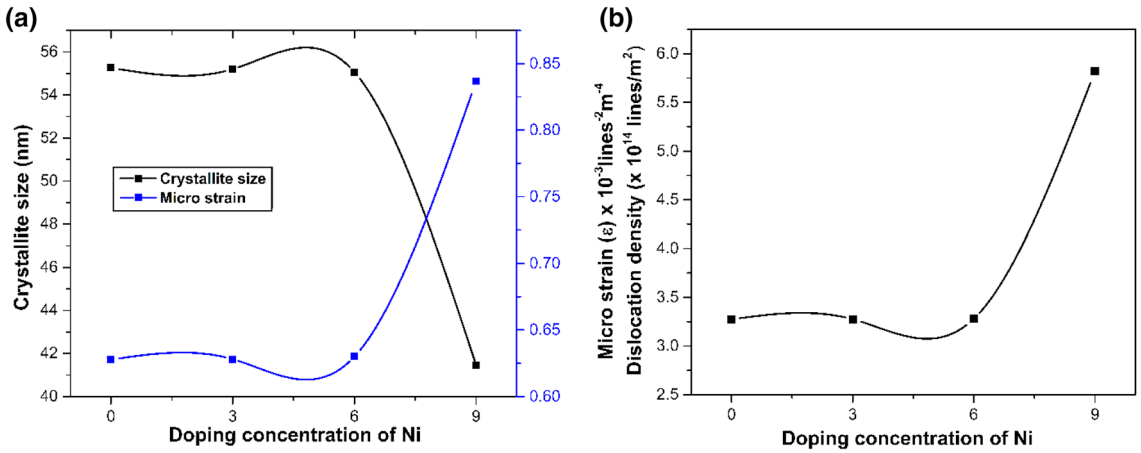

Fig. 3 **a** Crystallite size and microstrain for different doping concentrations from 0 to 9 wt.% of Ni-doped MoO_3 films. **b** The dislocation density of $NiMoO_3$ films

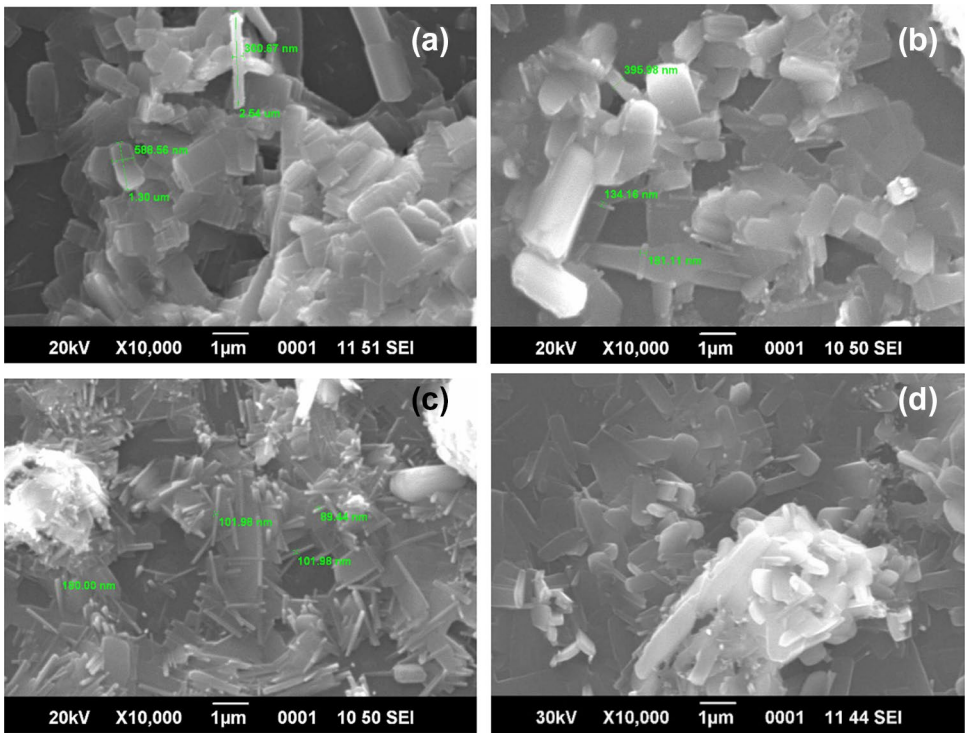

Fig. 4 Surface morphological images for **a** 0, **b** 3, **c** 6 and **d** 9 wt.% of Ni-doped MoO_3 thin films

enhances the electrical properties of the present films due to higher surface to volume ratio and charge accommodation ability. The results suggest that the Ni doping effectively changes the morphologies of the MoO_3 thin film in the present method of JNS pyrolysis.

3.4 Elemental analysis

The stoichiometric ratio of the JNS-coated $NiMoO_3$ thin films is confirmed by the EDX spectra. The pure MoO_3 thin film was discussed in earlier reports [14, 15]. The EDX spectra for Ni-doped MoO_3 thin films for different Ni doping concentrations of 3, 6 and 9 wt.% are shown in Fig. 5a–c. The EDX spectra reveal that the elements of Ni, Mo and O are present in the prepared samples by JNS pyrolysis. As the doping concentration of Ni increases, the atomic percentage of Ni increases and O decreases in the present study. Table 2 shows that the atomic percentage of Ni and Mo increases and O decreases with increasing the doping concentration of Ni.

3.5 Electrical characterization

3.5.1 DC conductivity

The DC electrical conductivity measurement of the different doping concentrations of Ni doped MoO_3 films is taken under varying temperatures from 30 to 150 °C in an increase of 20 °C by Keithley electrometer 6517-B through two-probe setup. The values of current are measured for the constant potential from 10 to 100 V in an increase of 10 V. For different Ni doping concentrations of 0, 3, 6 and 9 wt.% of $NiMoO_3$ thin films, the current–voltage (I–V) characterization has been taken and shown in Fig. 6a–d. Figure 6 shows that for the corresponding voltages (i.e., x-axis), the current values (y-axis) are directly proportional in nature for each temperature condition (30–150 °C).

The following relation (6) is used to calculate the DC conductivity (σ) [14, 15]:

$$\sigma = \left(\frac{I}{V}\right) \times \left(\frac{d}{A}\right), \tag{6}$$

where 'I'—current, 'V'—applied voltage, 'd'—inter-probe distance and 'A'—cross-sectional area of the film.

The conductivity of Ni-doped MoO_3 is increased by increasing Ni doping concentration from 0 to 9 wt.% and also each doping concentration of Ni-doped MoO_3 films shows the increase in conductivity owing to increase in temperature of 30–150 °C (Fig. 7). This result confirmed that the Ni-doped MoO_3 films are showing the semiconducting nature. In general, Semiconductors behave as an insulator at low temperatures and at higher temperatures, they act as conductors because the electrons around the atoms of semiconductor can break away from their covalent bond and move freely about the lattice. From Fig. 7 (inset), the average conductivity values are 9.144×10^{-13}, 2.716×10^{-12}, 4.121×10^{-12} and 5.026×10^{-12} S/cm for

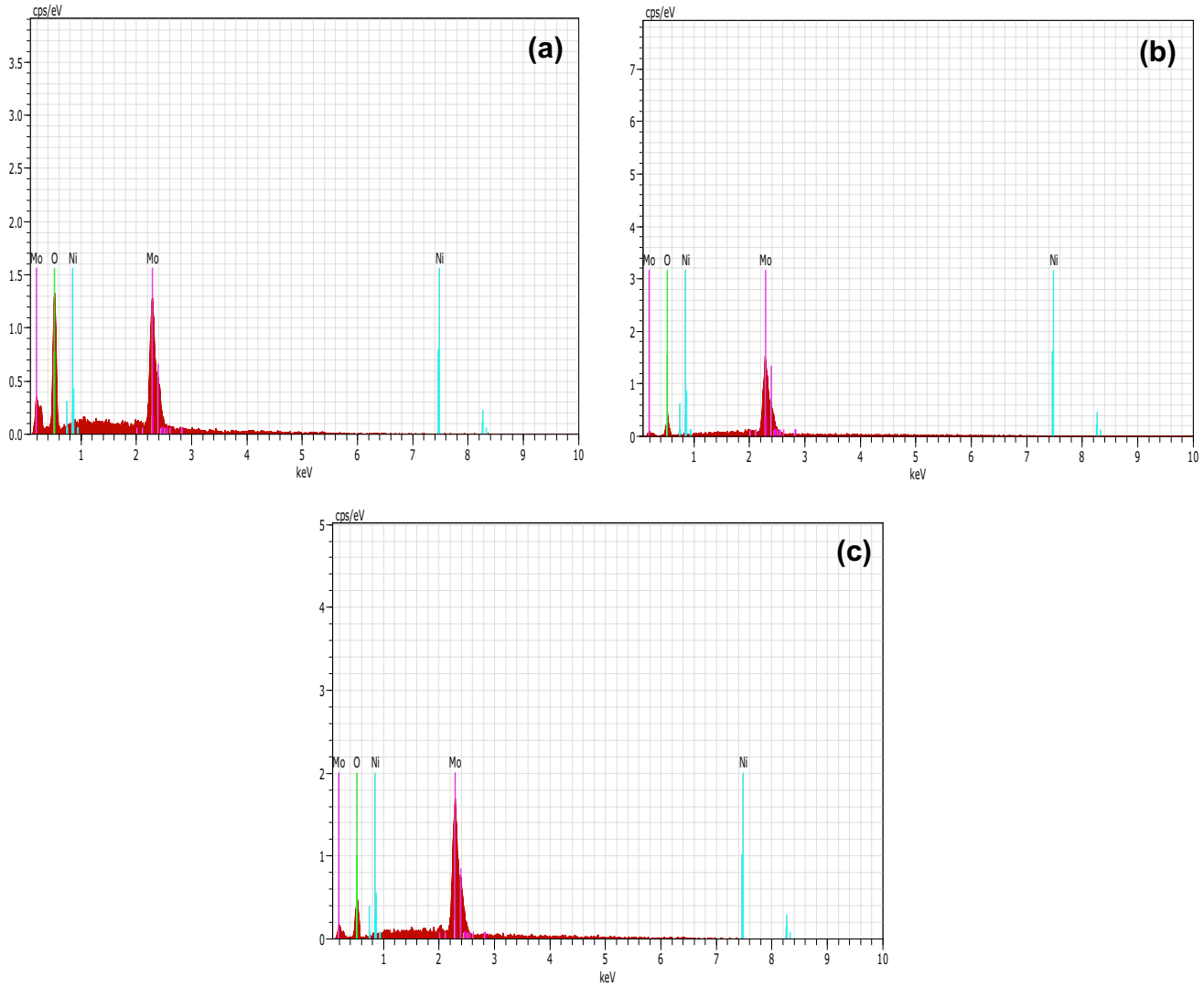

Fig. 5 EDX spectra for **a** 3, **b** 6 and **c** 9 wt.% of Ni-doped MoO_3 thin films

Table 2 The atomic percentage of $NiMoO_3$ films

Ni doping concentrations (wt.%)	Atomic ratio (%)		
	Ni	Mo	O
0	–	28.48	71.52
3	0.83	29.04	70.13
6	1.13	29.62	69.25
9	1.50	30.84	67.66

the corresponding Ni doping concentrations of 0, 3, 6 and 9 wt.% on Ni-doped MoO_3 films. The result suggests that the conductivity of Ni-doped MoO_3 films is increased by increasing the doping concentration of Ni due to the oxygen vacancies in the grown thin films [30] in the present study of JNS pyrolysis.

3.5.2 The diode parameters of n-$NiMoO_3$/p-Si

The n-$NiMoO_3$/p-Si diodes were fabricated for varying Ni doping concentrations of 0, 3, 6 and 9 wt.%) by JNS pyrolysis technique. The forward to the reverse bias current of the prepared diodes is taken for the corresponding voltage from − 4 to + 4 V in darkness and under a light illumination of halogen lamp as shown in Fig. 8a–d. The measurement conditions of the fabricated n-$NiMoO_3$/p-Si diodes are summarized in Table 3. According to Fig. 8a–d, the prepared diodes perform like a good conductor when a forward bias voltage is applied and like a good insulator when a reverse bias voltage is applied. So when the positive voltage is applied across the anode to the cathode, the diode does conduction of forward current instantly. This result implies that the nature of ideal diode behavior is observed for prepared diodes. Figure 9a–d illustrates the semi-log plot of current density (ln *J*) versus

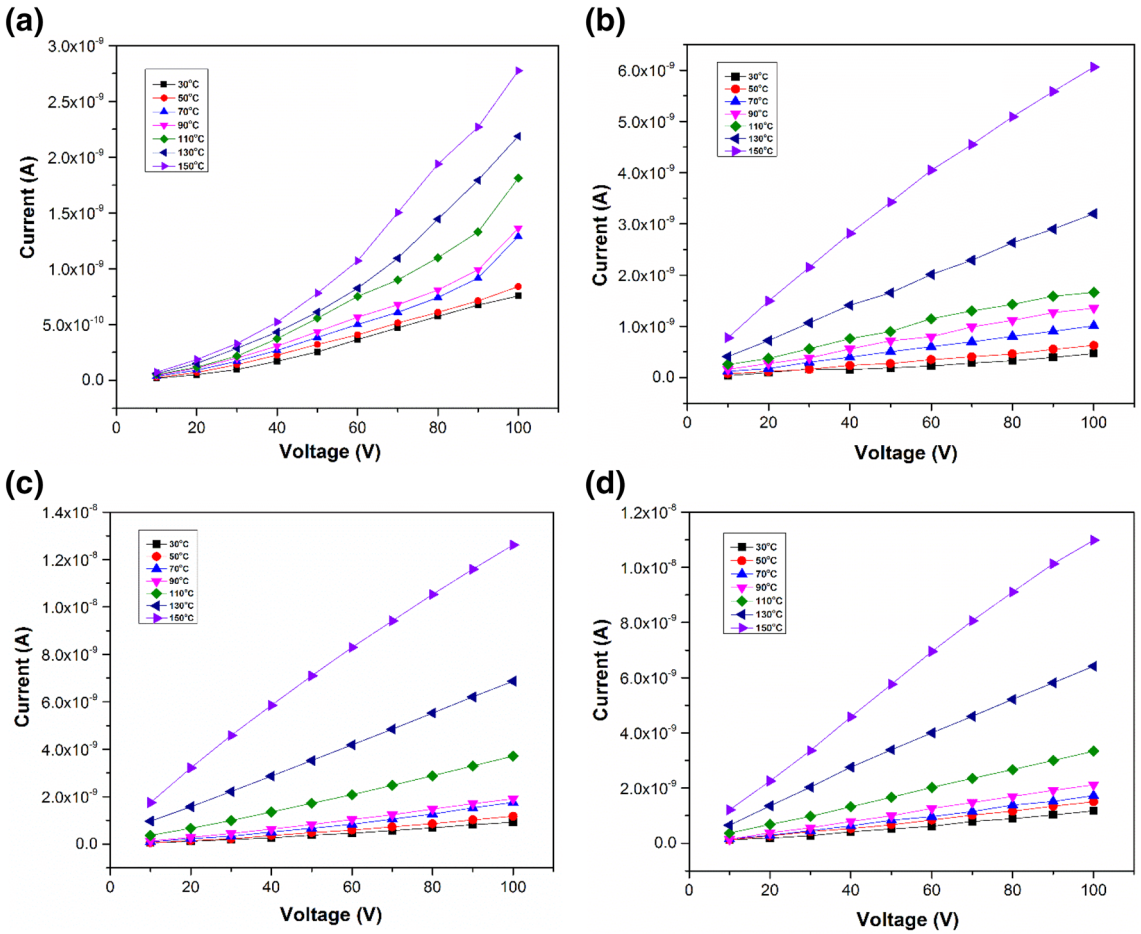

Fig. 6 *I–V* characterization for **a** 0, **b** 3, **c** 6 and **d** 9 wt.% of Ni-doped MoO_3 thin films under different measuring temperature

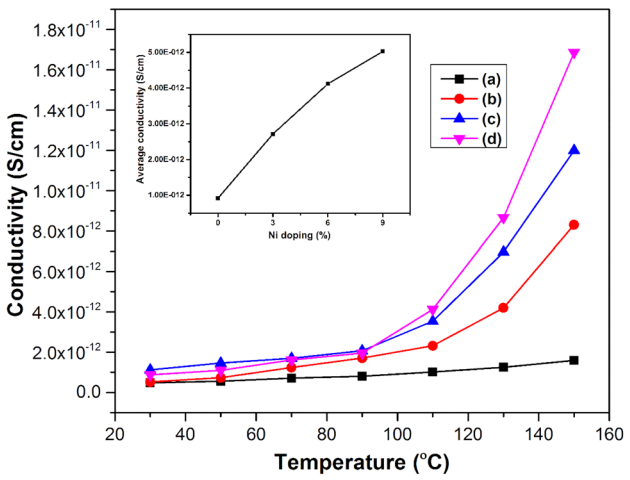

Fig. 7 The conductivity for **a** 0, **b** 3, **c** 6 and **d** 9 wt.% of Ni-doped MoO_3 thin films and average conductivity (Inset)

voltage (*V*). The n-$NiMoO_3$/p-Si diodes show good rectification behavior. The current density of the n-$NiMoO_3$/p-Si diodes is calculated by the thermionic emission theory (TE) as follows (7) [30, 31]:

$$J = J_0 \exp\left(\frac{qV}{nKT} - 1\right), \tag{7}$$

where 'J_0'—reverse saturation current density, 'q'—electron charge, 'V'—applied voltage, 'n'—ideality factor, 'K'—Boltzmann constant and 'T'—absolute temperature.

The ideality factor of the diode is determined from the slope and the intercept of the semi-log forward bias of *J–V* plot for $V \geq 3kT/q$ using Eq. (7).

The Φ_b and n are calculated using the following relations (8, 9) [31] and the values are shown in Table 4:

$$n = \frac{q}{KT}\frac{dV}{d(\ln J)}, \tag{8}$$

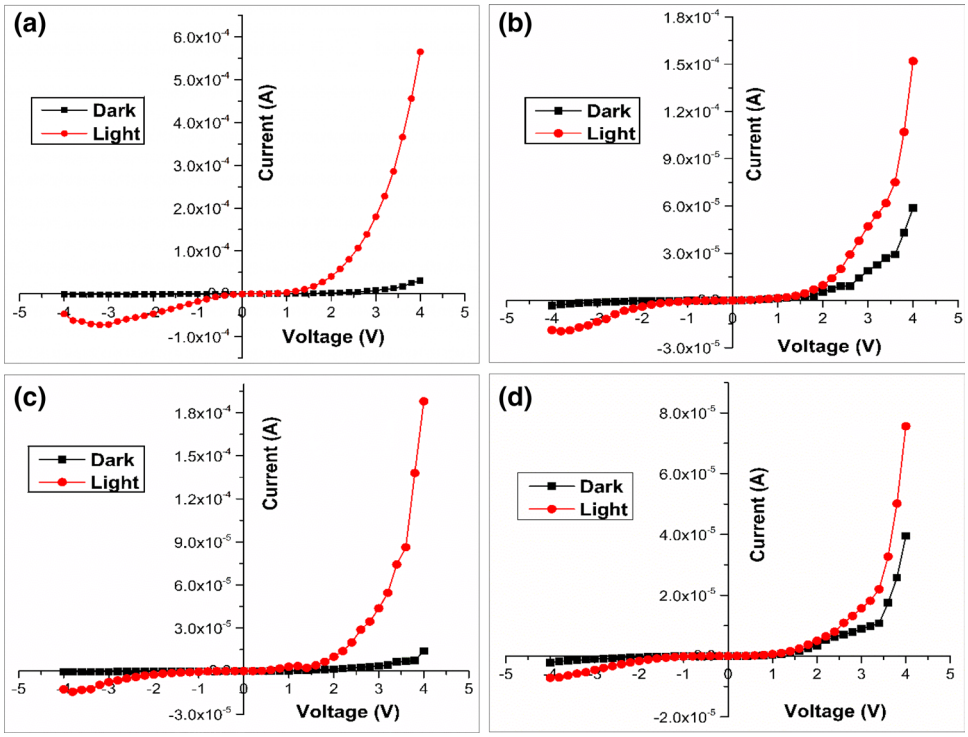

Fig. 8 *I–V* of n-$NiMoO_3$/p-Si diodes in darkness and under light illumination for different doping concentration of nickel of **a** 0, **b** 3, **c** 6 and **d** 9 wt.%

Table 3 Measurement conditions of the fabricated n-$NiMoO_3$/p-Si diodes in under light

Parameters	Values
Make	OSRAM lighting private limited, India
Lamp	Halogen
Power	1000 W
Wavelength	320 nm
Intensity	100 mW/cm^2
Distance between the sample and lamp	20 cm

$$\Phi_b = \frac{KT}{q}\ln\left(\frac{A^*T^2}{J_0}\right), \tag{9}$$

where A^*—Richardson constant.

In *J–V* method, the obtained *n* values of n-$NiMoO_3$/p-Si diodes for different doping concentrations of Ni from 0 to 9 wt.% have decreased from 7.19 to 5.03 in darkness and 5.16 to 4.89 under light illumination of a halogen lamp. The minimum n values of 5.03 and 4.89 are observed in dark and under light illumination for 9 wt.% of Ni-doped MoO_3 diode. The result agrees well with the reported work of pure p-NiO/n-Si p–n junction diode application [32].

The obtained *n* values mainly depend on the conversion efficiency of p-Si and the absorption of n-$NiMoO_3$ thin film layer including its thickness [33]. In an ideal p–n diode, the n value is equal to one, but here we observed that the *n* values are higher than that of an ideal p–n diode. This non-ideal behavior of n-$NiMoO_3$/p-Si diodes may be owing to the interfacial thin native layer of SiO_2 presence in between the electrode and Si wafer or recombination of charge in the space charge region [31, 34] and inhomogeneities of barrier [35].

Under ON (light illumination) and OFF (dark) conditions of halogen lamp, the current (*I*) values through the n-$NiMoO_3$/p-Si diodes (Ni—0, 3, 6 and 9 wt.%) were measured for 90 s under light illumination and for 90 s in the darkness of total time dilation of 0 to 900 s. In each illumination and darkness of measurements during the time of 0 to 900 s, the *I* values are denoted for every 30 s (Fig. 10a–d. From Fig. 10, the diodes under light illumination provide high current values than in the darkness. The results suggest that the diodes under light illumination produce a number of charge carriers, which increase the flow of current. From ON and OFF conditions, the prepared n-$NiMoO_3$/p-Si diodes have shown the photo-conducting behavior [15, 37]. To study the effect of R_s, *n* and Φ_b for the diodes, Cheung and Cheung have developed the functions [37] as follows (10–12):

$$\frac{dV}{d(\ln J)} = JR_s + n\left(\frac{kT}{q}\right), \tag{10}$$

$$H(J) = V - \left(\frac{nkT}{q}\right)\ln\left(\frac{J}{A^*T^2}\right), \tag{11}$$

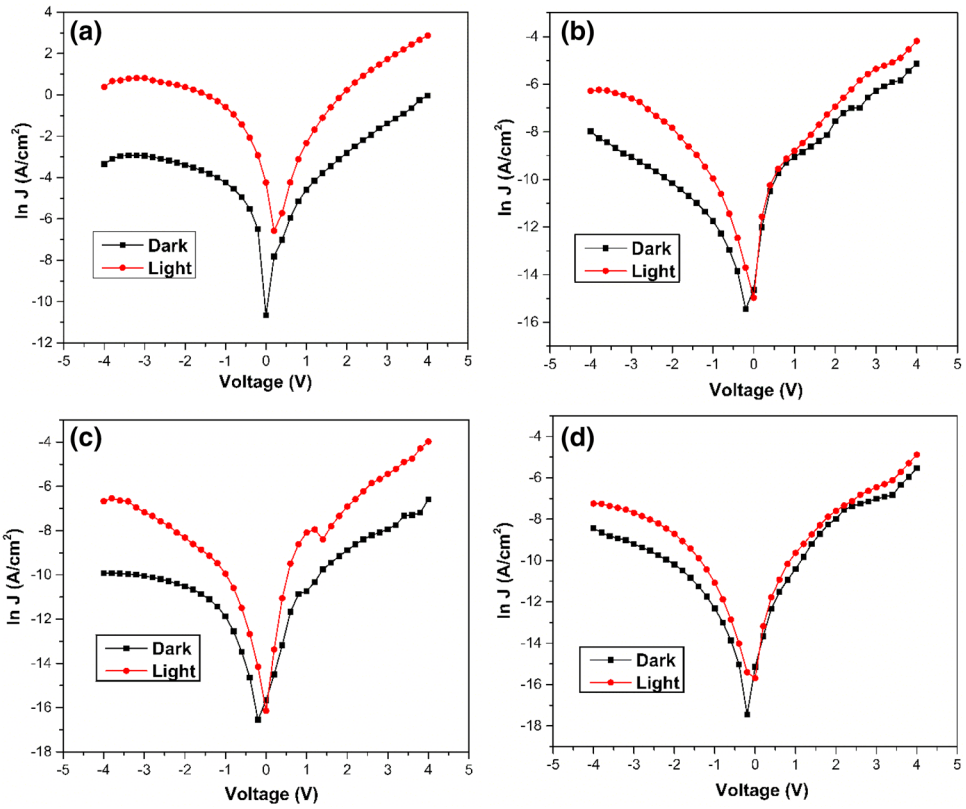

Fig. 9 ln J vs. voltage plot of n-NiMoO_3/p-Si diodes in darkness and under light illumination for different doping concentration of nickel of **a** 0, **b** 3, **c** 6 and **d** 9 wt.%

Table 4 Diode parameters of n, Φ_b and R_s from different methods of J–V, Cheung's and Norde

Ni doping concentration (wt.%)	J–V method				Cheung's method								Norde function			
					dV/d(ln J) vs J				$H(J)$ vs J							
	Φ_b (eV)		n		R_s (Ω)		n		R_s (Ω)		Φ_b (eV)		Φ_b (eV)		R_s (KΩ)	
	Dark	Light	Dark	Light	Dark	Light	Dark	Light	Dark	Light	Dark	Light	Dark	Light	Dark	Light
0	0.75	0.59	7.19	5.16	27.71	3.349	7.01	5.17	316.83	26.189	0.92	0.92	0.95	0.92	0.243	5.598
3	0.80	0.81	5.79	5.48	17.50	5.739	5.94	5.37	348.25	156.50	0.93	0.94	0.94	0.95	0.674	6.591
6	0.82	0.83	5.78	5.47	25.35	7.780	5.93	5.36	255.23	95.400	0.92	0.98	0.92	0.91	0.696	10.60
9	0.83	0.84	5.03	4.89	30.84	13.59	5.06	4.79	246.33	84.960	0.82	0.90	0.88	0.87	0.966	15.80

and $H(J)$ is re-written as

$$H(J) = JR_s + n_b, \tag{12}$$

Figure 11a–d depicts plots of dV/d(ln J) versus J for different doping concentrations of Ni (0, 3, 6 and 9 wt.%) on n-NiMoO_3/p-Si diodes in darkness and under illumination. Using the relation (10), a straight line is drawn on dV/d(ln J) versus J plot (Fig. 11), which gives the values of nkT/q and the R_s value is obtained from the axis of dV/d(ln J) and slope of the dV/d(ln J). From Fig. 12, another determination of R_s and $n\Phi_b$ is found from the slope and plots of H(J) versus J using the relation (12). Using Cheung and Cheung method, the values of n, R_s and Φ_b are calculated and listed in Table 4. From Table 4, the Cheung's method reveals that the minimum n values are found to be 5.06 and 4.79 in darkness and under light illumination for 9 wt.% Ni-doped MoO_3 diode.

Moreover, an alternative method was used to determine the values of Φ_b and R_s by Norde [38]. Figure 13a–d shows the plot of $F(V)$ versus voltage of n-NiMoO_3/p-Si diodes for the different doping concentrations of Ni under the illumination of light and in darkness.

This altered function of Norde method is determined as follows (13–15) [38]:

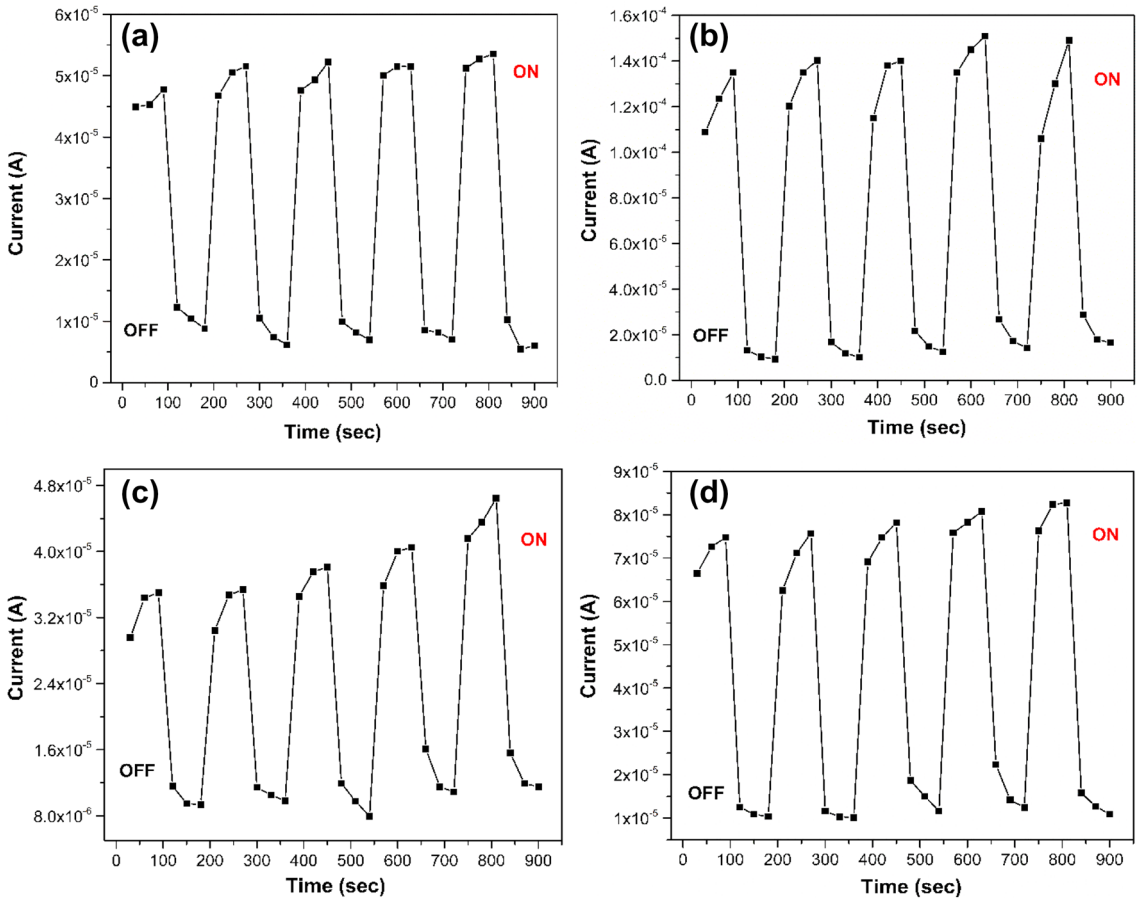

Fig. 10 *I–V* measurements of n-$NiMoO_3$/p-Si diodes for different doping concentration of nickel of **a** 0, **b** 3, **c** 6 and **d** 9 wt.% under ON–OFF conditions of a halogen lamp

$$F(V) = \frac{V}{\gamma} - \frac{kT}{q}\left(\frac{J(V)}{A^{*}T^{2}}\right), \tag{13}$$

where 'γ'—integer (dimensionless) > n, '$J(V)$'—obtained from the J–V curve.

The Φ_b of n-$NiMoO_3$/p-Si diode is calculated by the following relation (14):

$$\Phi_b = F(V_0) + \frac{V_0}{\gamma} - \frac{kT}{q}, \tag{14}$$

where '$F(V_0)$'—the minimum value is taken from the plot of $F(V)$ versus voltage plot (Fig. 13) and 'V_0'—corresponding voltage.

Using Norde function, R_s is determined by the following relation (15):

$$R_s = \frac{kT(\gamma - n)}{qJ_{min}}, \tag{15}$$

where 'J_{min}'—minimum value of current density for V_0.

The obtained values of Φ_b and R_s using the Norde function are given in Table 4: the R_s values are increasing and Φ_b values are decreasing with increasing the doping concentrations of Ni on n-$NiMoO_3$/p-Si diode both in the darkness and under the illumination of light as shown in Table 4. The values of R_s using Norde method are comparatively higher than the Cheung's method and Φ_b values vary in the methods of J–V, Cheung's method and Norde function. This results suggest that the variations in Φ_b values are owing to the extraction through different regions of the forward bias of the J–V curve [39]. Moreover, in the forward bias region of the J–V curve, Cheung's method is developed especially for the non-linear region, but the Norde function is applied to the whole region [2, 40].

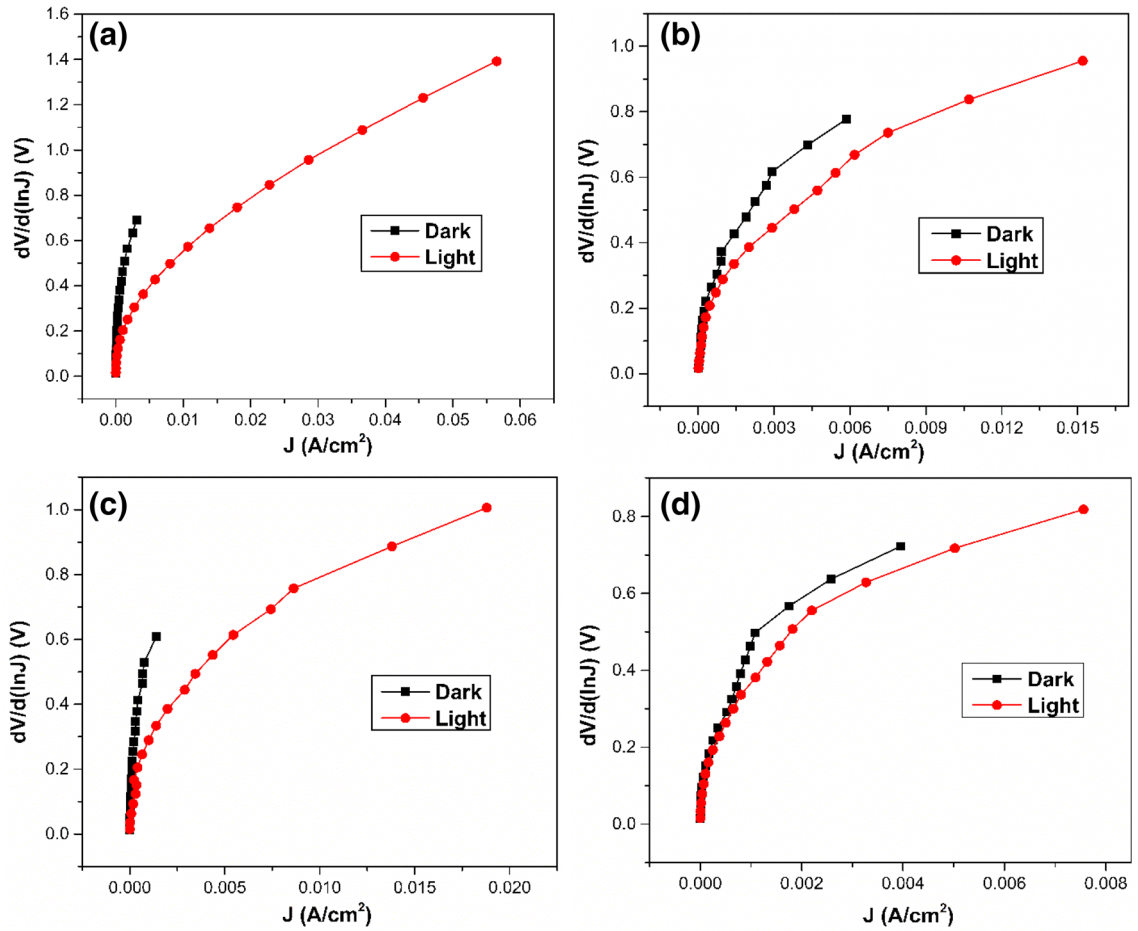

Fig. 11 d*V*/d(ln *J*) vs. *J* of n-$NiMoO_3$/p-Si diodes in darkness and under light illumination for different doping concentration of nickel of **a** 0, **b** 3, **c** 6 and **d** 9 wt.%

4 Conclusion

The JNS pyrolysis technique was used to fabricate the $NiMoO_3$ thin films and n-$NiMoO_3$/p-Si diodes at 500 °C for different doping concentrations of Ni from 0 to 9 wt.%. The structural study of XRD pattern shows that the prepared $NiMoO_3$ films are exhibited an orthorhombic structure in polycrystalline nature. A decrease in crystallite size from 55.26 to 41.45 nm and an increase in microstrain from 0.62×10^{-3} to 0.83×10^{-3} lines^{-2} m^{-4} were observed with increasing Ni dopant. From the morphological reports of SEM, the increasing of Ni doping strongly disturbs the surface morphology of the prepared samples. Elemental analysis of EDX spectra confirms that the elements of Ni, Mo and O are presented in the JNS pyrolysis technique. Using UV–vis spectra, the optical properties of $NiMoO_3$ films were studied. The minimum absorbance and band gap of 2.25 eV were identified for 9 wt.% Ni-doped MoO_3 film. The electrical measurement of *I–V* reveals that the 9 wt.% Ni-doped MoO_3 film provides a maximum conductivity of 5.026×10^{-12} S/cm. From the diode characterization, in darkness and under light illumination, 9 wt.% of n-$NiMoO_3$/p-Si diode shows that the minimum *n* values of 5.03 and 4.89 using *J–V* method and 5.06 and 4.79 using Cheung's method are obtained. From all the above results, we infer that the 9 wt.% of n-$NiMoO_3$/p-Si diode is highly suitable for ON/OFF switching device application. The above results show that the prepared devices may be suitable for photo-detector applications.

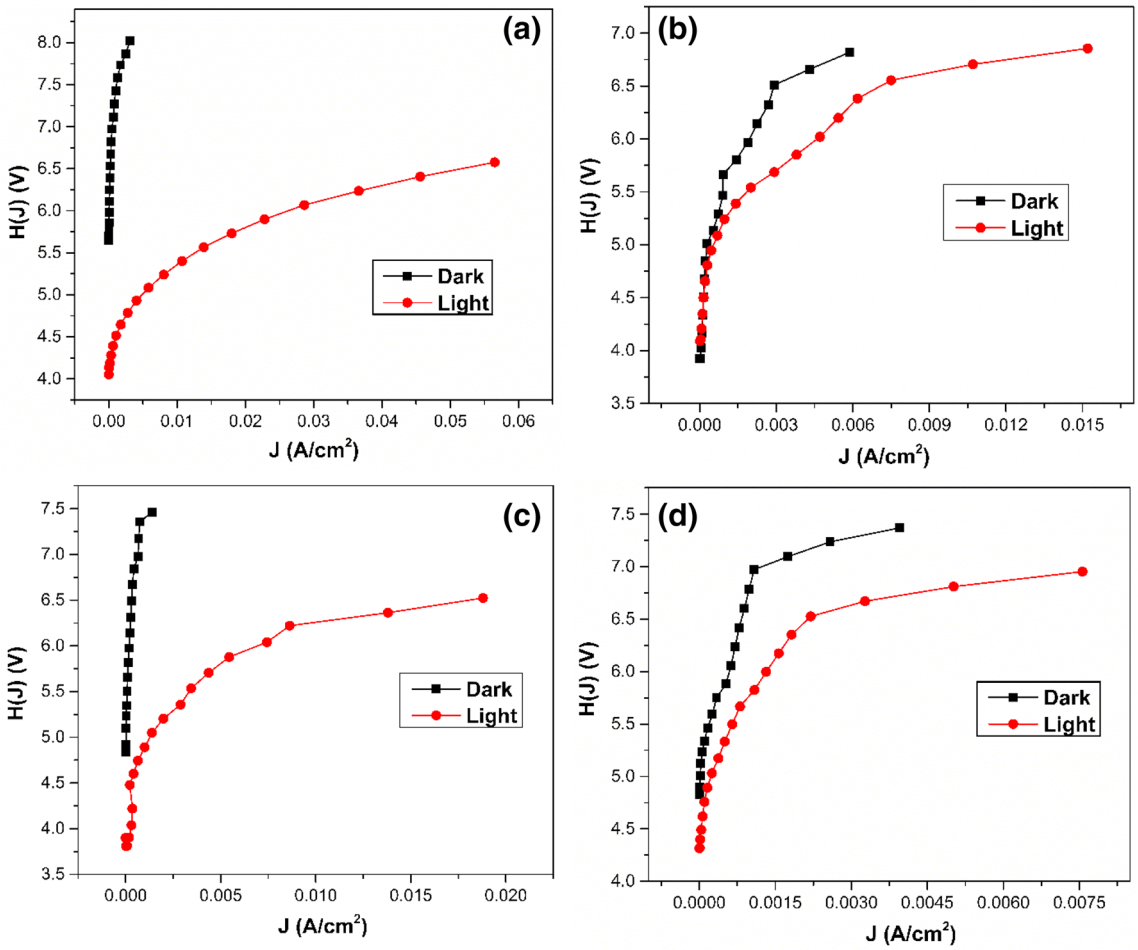

Fig. 12 *H*(*J*) vs. *J* of n-$NiMoO_3$/p-Si diodes in darkness and under light illumination for different doping concentration of nickel of **a** 0, **b** 3, **c** 6 and **d** 9 wt.%

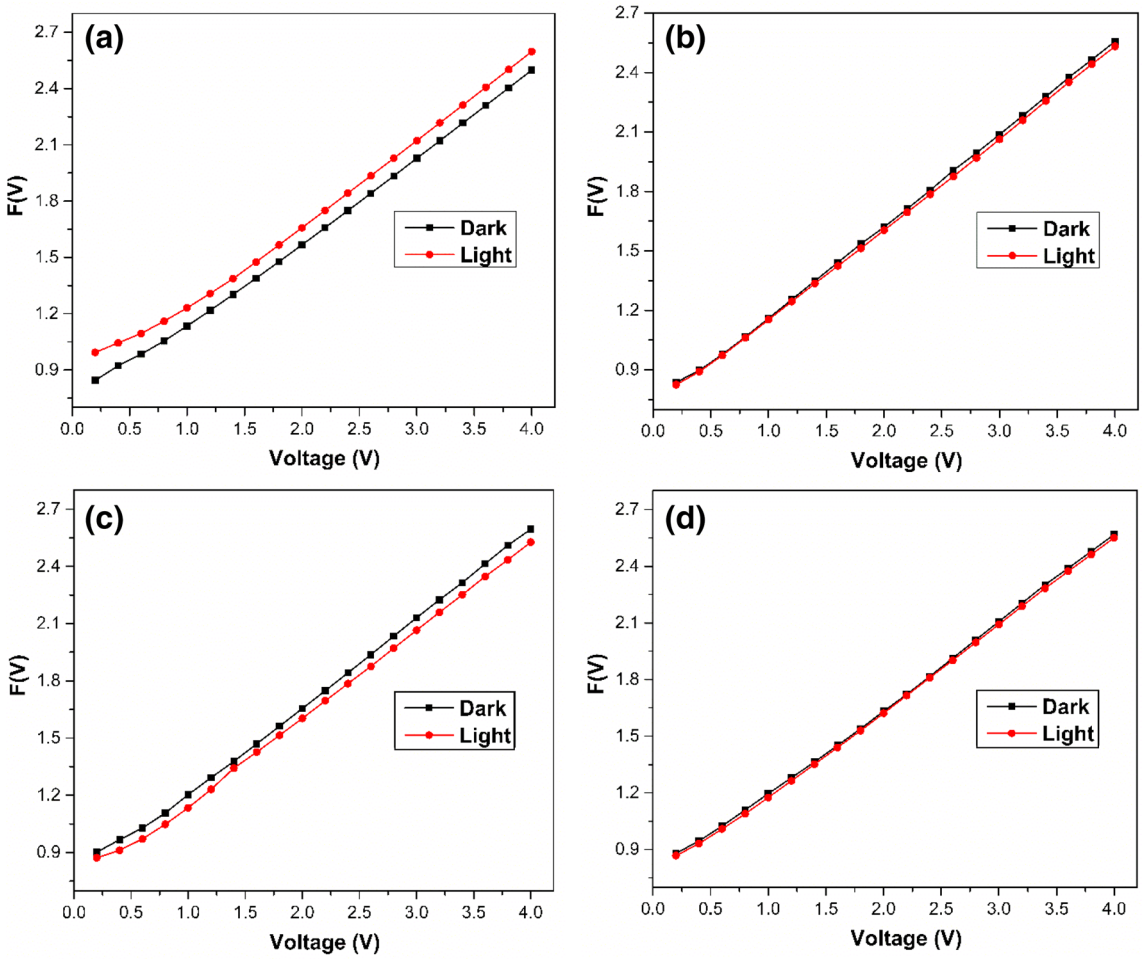

Fig. 13 *F*(*V*) vs. voltage of n-NiMoO_3/p-Si diodes in darkness and under light illumination for different doping concentration of nickel of **a** 0, **b** 3, **c** 6 and **d** 9 wt.%

Acknowledgements The authors gratefully acknowledge the financial support from the DST, Government of India, for the major research project (EMR/2016/007874). Author M. Shkir also thankful to the Deanship of Scientific Research at King Khalid University, KSA for funding this work through research groups program under grant number R.G.P. 2/41/40.

Compliance with ethical standards

Conflict of interest The authors declare that they have no conflict of interest.

References

1. G. Wang, T. Jiu, P. Li, J. Li, C. Sun, F. Lu, J. Fang, Preparation and characterization of MoO_3 hole-injection layer for organic solar cell fabrication and optimization. Sol. Energy Mater. Sol. Cells **120**, 603–609 (2014)
2. Q. Fu, J. Chen, C. Shi, D. Ma, Room-temperature sol–gel derived molybdenum oxide thin films for efficient and stable solution-processed organic light-emitting diodes. ACS Appl. Mater. Interfaces. https://doi.org/10.1021/am4007319.
3. R. Pandeeswari, B.G. Jeyaprakash, Nanostructured α-MoO_3 thin film as a highly selective TMA sensor. Biosens. Bioelectron. (2013). https://doi.org/10.1016/j.bios.2013.09.057
4. T.N. Lin, Y.H. Lin, C.T. Lee, S. Han, K.W. Weng, Electrochromic properties of bipolar pulsed magnetron sputter deposited tungsten-molybdenum oxide films. Thin Solid Films (2015). https://doi.org/10.1016/j.tsf.2014.12.036
5. L. Zheng, Y. Xu, D. Jin, Y. Xie, Novel metastable hexagonal MoO_3 nanobelts: synthesis, photochromic and electrochromic properties. Chem. Mater. **21**, 5681–5690 (2009)
6. C.L. Liu, Y. Wang, C. Zhang, X.S. Li, W.S. Dong, In situ synthesis of α-MoO_3/graphene composites as anode materials for lithium ion battery. Mater. Chem. Phys. **143**, 1111–1118 (2014)
7. P. Vivek, J. Chandrasekaran, R. Marnadu, S. Maruthamuthu, V. Balasubramani, Incorporation of Ba^{2+} ions on the properties of MoO_3 thin films and fabrication of positive photo-response Cu/Ba–MoO_3/p-Si structured diodes. Superlattices Microstruct **133**, 106197 (2019)
8. K.A. Gesheva, T. Ivanova, A low-temperature atmospheric pressure CVD process for growing thin films of MoO_3 and

MoO_3-WO_3 for electrochromic device applications. Chem. Vap. Depos. **12**, 231–238 (2006)
9. K. Galatsis, Y.X. Li, W. Wlodarski, K. Kalantar-zadeh, Sol-gel prepared MoO_3-WO_3 thin films for O_2 gas sensing. Sens. Actuators B **77**, 478–483 (2001)
10. B. Kannan, R. Pandeeswari, B.G. Jeyaprakash, Influence of precursor solution volume on the properties of spray deposited α-MoO_3 thin films. Ceram. Int. **40**, 5817–5823 (2014)
11. M.B. Rahmani, S.H. Keshmiri, J. Yu, A.Z. Sadek, L. Al-Mashat, A. Moafi, K. Latham, Y.X. Li, W. Wlodarski, K. Kalantar-zadeh, Gas sensing properties of thermally evaporated lamellar MoO_3. Sens. Actuators B **145**, 13–19 (2010)
12. K. Gesheva, A. Cziraki, T. Ivanova, A. Szekeres, Structure and composition of thermally annealed Mo- and W-based CVD metal oxide thin films. Thin Solid Films **492**, 322–326 (2005)
13. N. Sethupathi, P. Thirunavukkarasu, V.S. Vidhya, R. Thangamuthu, G.V.M. Kiruthika, K. Perumal, H.C. Bajaj, M. Jayachandran, Deposition and optoelectronic properties of ITO (In2O3–Sn) thin films by jet nebulizer spray (JNS) pyrolysis technique. J. Mater. Sci.: Mater Electron. **23**, 1087–1093 (2012)
14. M. Balaji, J. Chandrasekaran, M. Raja, Role of substrate temperature on MoO_3 thin films by the JNS pyrolysis technique for p-n junction diode application. Mater. Sci. Semicond. Process. **43**, 104–113 (2016)
15. M. Balaji, J. Chandrasekaran, M. Raja, S. Rajesh, Structural, optical and electrical properties of Ru doped MoO_3 thin films and its p–n diode application by JNS pyrolysis technique. J. Mater. Sci.: Mater. Electron. (2016). https://doi.org/10.1007/s10854-016-5300-0
16. R.K. Mishra, P.P. Sahay, Zn-doped and undoped SnO_2 nanoparticles: a comparative structural, optical and LPG sensing properties study. Mater. Res. Bull. **47**, 4112–4118 (2012)
17. M. Raja, J. Chandrasekaran, M. Balaji, The structural, optical and electrical properties of spin coated WO_3 thin films using organic acids. Silicon (2016). https://doi.org/10.1007/s12633-016-9413-0
18. M. Dhanasankar, K.K. Purushothaman, G. Muralidharan, Optical, structural and electrochromic studies of molybdenum oxide thin films with nanorod structure. Solid State Sci. **12**, 246–251 (2010)
19. E. Burstein, Anomalous optical absorption limit in InSb. Phys. Rev. **93**, 632–633 (1954)
20. G. Turgut, E.F. Keskenler, S. Aydin, E. Sonmez, S. Dogan, B. Duzgun, M. Ertugrul, Effect of Nb doping on structural, electrical and optical properties of spray deposited SnO_2 thin films. Superlattices Microstruct. **56**, 107–116 (2013)
21. Y. Huang, G. Li, J. Feng, Q. Zhang, Investigation on structural, electrical and optical properties of tungsten-doped tin oxide thin films. Thin Solid Films **518**, 1892–1896 (2010)
22. X. Zhao, Z. Wu, D. Guo, W. Cui, P. Li, Y. An, L. Li, W. Tang, Growth and characterization of α-phase $Ga_{2-x}Sn_xO_3$ thin films for solar-blind ultraviolet applications. Semicond. Sci. Technol. **31**(1–6), 065010 (2016)
23. A.R. Babar, P.R. Deshamukh, R.J. Deokate, D. Haranath, C.H. Bhosale, K.Y. Rajpure, Gallium doping in transparent conductive ZnO thin films prepared by chemical spray pyrolysis. J. Phys. D: Appl. Phys. **41**(1–6), 135404 (2008)
24. D. Zhou, F. Shi, D. Xie, D.H. Wang, X.H. Xia, X.L. Wang, C.D. Gu, J.P. Tu, Bi-functional Mo-doped WO_3 nanowire array electrochromism-plus electrochemical energy storage. J. Colloid Interface Sci. (2015). https://doi.org/10.1016/j.jcis.2015.11.068
25. M. Thambidurai, N. Muthukumarasamy, S. Agilan, N. Murugan, N. Sabari Arul, S. Vasantha, R. Balasundaraprabhu, Studies on optical absorption and structural properties of Fe doped CdS quantum dots, Solid State Sci. **12**, 1554–1559 (2010).
26. P. Scherrer, Bestimmung der Grösse und der inneren Struktur von Kolloidteilchen mittels Rontgenstrahlen. Nachr. Ges. Wiss. Gottingen **26**, 98 (1918)
27. V. Madhavi, P. Jeevan Kumar, P. Kondaiah, O.M. Hussain, S. Uthanna, Effect of molybdenum doping on the electrochromic properties of tungsten oxide thin films by RF magnetron sputtering. Ionics (2014). https://doi.org/10.1007/s11581-014-1073-8
28. K.J. Lethy, D. Beena, V.P. Mahadevan Pillai, V. Ganesan, Band gap renormalization in titania modified nanostructured tungsten oxide thin films prepared by pulsed laser deposition technique for solar cell applications, J. Appl. Phys. 104 (2008) 033515(1–12).
29. V. Nirupama, M. ChandraSekhar, T.K. Subramanyam, S. Uthanna, Structural and electrical characterization of magnetron sputtered MoO3 thin films. J. Phys. Conf. Ser. **208**(1–6), 012101 (2010)
30. R. Marnadu, J. Chandrasekaran, P. Vivek, V. Balasubramani, S. Maruthamuthu, Impact of phase transformation in WO_3 thin films at higher temperature and its compelling interfacial role in Cu/WO_3/p-Si structure schottky barrier diodes. Z. Phys. Chem. (2019). https://doi.org/10.1515/zpch-2018-1289
31. R. Marnadu, J. Chandrasekaran, M. Raja, M. Balaji, S. Maruthamuthu, P. Balraju, Influence of metal work function and incorporation of Sr atom on WO3thin films for MIS and MIM structured SBDs. Superlattices Microstruct. **119**, 134–149 (2018)
32. J. Saju, O.N. Balasundaram, Optimization and characterization of NiO thin films prepared via NSP technique and its p–n junction diode application. Mater. Sci. Poland **37**(3), 338–346 (2019)
33. L.R. Canfield, R. Vest, T.N. Woods, R. Korde, Silicon photodiodes with integrated thin film filters for selective bandpasses in the extreme ultraviolet. Ultraviolet Tech. V **2282**, 31–38 (1994)
34. R. Marnadu, J. Chandrasekaran, S. Maruthamuthu, V. Balasubramani, P. Vivek, R. Suresh, Ultra-high photoresponse with superiorly sensitive metal-insulator-semiconductor (MIS) structured diodes for UV photodetector application. Appl Surf Sci **480**, 308–322 (2019)
35. R. Marnadu, J. Chandrasekaran, M. Raja, M. Balaji, V. Balasubramani, Impact of Zr content on multiphase zirconium–tungsten oxide (Zr–WOx) films and its MIS structure of Cu/Zr–WOx/p-Si Schottky barrier diodes. J. Mater. Sci. Mater Electron. **29**, 2618–2627 (2018)
36. N. Senthilkumar, M. SethuRaman, J. Chandrasekaran, R. Priya, M. Chavali, R. Suresh, Effect of post-growth annealing on the structural, optical and electrical properties of V2O5 nanorods and its fabrication, characterization of V2O5/p-Si junction diode. Mater. Sci. Semicond. Process. **41**, 497–507 (2016)
37. S.K. Cheung, N.W. Cheung, Extraction of Schottky diode parameters from forward current-voltage characteristics. Appl. Phys. Lett. **49**, 85 (1986)
38. H. Norde, A modified forward *I–V* plot for Schottky diodes with high series resistance. J. Appl. Phys. **50**, 5052 (1979)
39. S. Karatas, Effect of series resistance on the electrical characteristics and interface state energy distributions of Sn/p-Si (MS) Schottky diodes. Microelectron. Eng. **87**, 1935–1940 (2010)
40. R.K. Gupta, K. Ghosh, P.K. Kahol, Temperature dependence of current-voltage characteristics of gold-strontium titanate thin film Schottky diode. Physica E **42**, 1509–1512 (2010)
41. M. Raja, J. Chandrasekaran, M. Balaji, P. Kathirvel, R. Marnadu, Influence of metal (M = Cd, In, and Sn) dopants on the properties of spin-coated WO3 thin films and fabrication of temperature dependent heterojunction diodes. J. Sol-Gel Sci Technol. (2020). https://doi.org/10.1007/s10971-019-05207-9